A SPECTRALLY ACCURATE NUMERICAL METHOD FOR COMPUTING THE RWA EXCITATIONS OF DIPOLAR BOSE-EINSTEIN CONDENSATES

QINGLIN TANG*, MANTING XIE†, YONG ZHANG‡§, AND YUQING ZHANG¶

Abstract. In this paper, we propose an efficient and robust numerical method to study the elementary excitation of dipolar Bose-Einstein condensates (BEC), which is governed by the Bogoliubov-de Gennes equations (BdGEs) with nonlocal dipole-dipole interaction, around the mean field ground state. Analytical properties of the BdGEs are investigated, which could serve as benchmarks for the numerical methods. To evaluate the nonlocal interactions accurately and efficiently, we propose a new Simple Fourier Spectral Convolution method (SFSC). Then, integrating SFSC with the standard Fourier spectral method for spatial discretization and Implicitly Restarted Arnoldi Methods (IRAM) for the eigenvalue problem, we derive an efficient and spectrally accurate method, named as SFSC-IRAM method, for the BdGEs. Ample numerical tests are provided to illustrate the accuracy and efficiency. Finally, we apply the new method to study systematically the excitation spectrum and Bogoliubov amplitudes around the ground state with different parameters in different spatial dimensions.

Key words. Bogoliubov-de Gennes excitations, dipolar Bose-Einstein condensates, Convolution-type nonlocal interaction, Fourier Spectral Convolution method

1. Introduction.

Since the realization of Bose-Einstein condensates (BEC) of dipolar quantum gases [2, 27, 38], we have witnessed unique and novel phenomenon, such as the roton-maxon spectrum[35, 41], the self-bound droplet state [23, 45] and the newfangled vortex lattice patterns [39], due to the fundamental anisotropic and long-range magnetic/electric dipole-dipole interatomic interaction. To understanding the stability of stationary states of a BEC, it is important to study its elementary excitations around the stationary states [35, 41]. The first experimental measurements of the lowest collective modes of BEC was carried out in [32]. Great efforts have been made to experimentally, theoretically and numerically study the collective excitations of BECs since then [20, 24, 28, 29, 33, 40, 41, 44, 50].

At temperature much lower than the critical value T_c, the properties of the BEC with long-range dipole-dipole interaction (DDI) are well characterized by the macroscopic complex-valued wave function $\psi(\boldsymbol{x}, t)$ whose evolution could be well governed by the three-dimensional (3D) Gross-Pitaevskii equation (GPE) with DDI term [5, 9, 10, 26, 53]. Moreover, the 3D GPE with some special highly anisotropic external potential could be reduced to an effective two-dimensional (2D) equation [15, 17, 10]. In dimensionless form, the d-dimensional ($d = 2$ or 3) GPE with DDI term could be

‡CORRESPONDING AUTHOR.

*School of Mathematics, State Key Laboratory of Hydraulics and Mountain River Engineering, Sichuan University, ChengDu 610064, China (qinglin_tang@scu.edu.cn). This research was supported by National Natural Science Foundation of China (No. 11971335) and the Institutional Research Fund from Sichuan University (No. 2020SCUNL110).

†Center for Applied Mathematics, Tianjin University, Tianjin 300072, China (mtxie@tju.edu.cn). This author's work was supported by the National Science Foundation of China (No. 12001402).

§Center for Applied Mathematics, Tianjin University, Tianjin 300072, China (Zhang_Yong@tju.edu.cn). This author's work was supported by the Fundamental Research Funds for the Central Universities (xxx)

¶Center for Applied Mathematics, Tianjin University, Tianjin 300072, China.

unified as [9, 17, 15]

$$i\partial_t\psi(\boldsymbol{x},t) = \left[-\frac{1}{2}\nabla^2 + V(\boldsymbol{x}) + \beta|\psi|^2 + \lambda\,\Phi\right]\psi, \quad \boldsymbol{x}\in\mathbb{R}^d, \quad t>0, \tag{1}$$

$$\Phi(\boldsymbol{x},t) := (U * |\psi|^2)(\boldsymbol{x},t), \tag{2}$$

$$\psi(\boldsymbol{x},0) = \psi_0(\boldsymbol{x}), \tag{3}$$

where t denotes time and $\boldsymbol{x} = (x,y)^T \in \mathbb{R}^2$ and/or $\boldsymbol{x} = (x,y,z)^T \in \mathbb{R}^3$ is the Cartesian coordinate vector, $*$ represents the convolution operator with respect to spatial variable. $V(\boldsymbol{x})$ is a real-valued external potential which is case-dependent and one common choice is the harmonic trapping potential which reads as

$$V(\boldsymbol{x}) = \frac{1}{2}\begin{cases} \gamma_x^2x^2 + \gamma_y^2y^2, & d=2,\\ \gamma_x^2x^2 + \gamma_y^2y^2 + \gamma_z^2z^2, & d=3. \end{cases} \tag{4}$$

Here, $\gamma_\alpha > 0$ ($\alpha = x,y,z$) are dimensionless constants proportional to the trapping frequency in ν-direction. Moreover, the dimensionless constant β and λ characterize respectively the short-range contact interaction and long-range DDI. The interaction kernel $U(\boldsymbol{x})$ reads as

$$U(\boldsymbol{x}) = \begin{cases} -\delta(\boldsymbol{x}) - 3\,\partial_{\boldsymbol{nn}}\left(\frac{1}{4\pi|\boldsymbol{x}|}\right), & \boldsymbol{x}\in\mathbb{R}^3,\\ -\frac{3}{2}\left(\partial_{\boldsymbol{n}_\perp\boldsymbol{n}_\perp} - n_3^2\nabla_\perp^2\right)\left(\frac{1}{2\pi|\boldsymbol{x}|}\right), & \boldsymbol{x}\in\mathbb{R}^2. \end{cases} \tag{5}$$

Here, $\boldsymbol{n} = (n_1,n_2,n_3)^T \in \mathbb{R}^3$ is a given unit vector representing the dipole moment, $\partial_{\boldsymbol{n}} = \boldsymbol{n}\cdot\nabla, \partial_{\boldsymbol{nn}} = \partial_{\boldsymbol{n}}(\partial_{\boldsymbol{n}})$, $\nabla_\perp = (\partial_x,\partial_y)^T$, $\boldsymbol{n}_\perp = (n_1,n_2)^T$ and $\partial_{\boldsymbol{n}_\perp} = \boldsymbol{n}_\perp\cdot\nabla_\perp, \partial_{\boldsymbol{n}_\perp\boldsymbol{n}_\perp} = \partial_{\boldsymbol{n}_\perp}(\partial_{\boldsymbol{n}_\perp})$.

The time dependent GPE (1)-(3) conserves two important quantities: the mass of the wave function

$$N(\psi(\cdot,t)) := \|\psi(\boldsymbol{x},t)\|^2 = \int_{\mathbb{R}^d}|\psi|^2\mathrm{d}\boldsymbol{x} \equiv N(\psi(\cdot,0)), \qquad t\ge 0, \tag{6}$$

and the energy *per particle*

$$E(\psi(\cdot,t)) = \int_{\mathbb{R}^d}\left[\frac{1}{2}|\nabla\psi|^2 + V(\boldsymbol{x})|\psi|^2 + \frac{\beta}{2}|\psi|^4 + \frac{\lambda}{2}\Phi|\psi|^2\right]\mathrm{d}\boldsymbol{x} \equiv E(\psi(\cdot,0)), t\ge 0. \tag{7}$$

Plug the ansatz $\psi(\boldsymbol{x},t) = e^{i\mu_s t}\phi_s(\boldsymbol{x})$ into (1), one obtains the following time-independent GPE for the stationary state $\phi_s(\boldsymbol{x})$:

$$\mu_s\phi_s(\boldsymbol{x}) = \left[-\frac{1}{2}\nabla^2 + V(\boldsymbol{x}) + \beta|\phi_s|^2 + \lambda\,(U*|\phi_s|^2)\right]\phi_s(\boldsymbol{x}), \quad \|\phi_s(\boldsymbol{x})\| = 1, \tag{8}$$

which is also a nonlinear eigenvalue problem. The corresponding eigenvalue $\mu_s\in\mathbb{R}$ is also called chemical potential which could be evaluated from $\phi_s(\boldsymbol{x})$ as follows

$$\mu_s = \int_{\mathbb{R}^d}\left[\frac{1}{2}|\nabla\phi_s|^2 + V(\boldsymbol{x})|\phi_s|^2 + \beta|\phi_s|^4 + \lambda\,(U*|\phi_s|^2)\,|\phi_s|^2\right]\mathrm{d}\boldsymbol{x}. \tag{9}$$

The ground state $\phi_g(\boldsymbol{x})$, which is the stationary state of the lowest energy, could also be interpreted as the global minimizer of the following non-convex minimization problem:

$$\phi_g(\boldsymbol{x}) = \arg\min_{\phi\in\mathcal{S}}\ \mathcal{E}(\phi), \tag{10}$$

with $\mathcal{S} := \{\phi(\boldsymbol{x}) \mid \|\phi\|^2 := \int_{\mathbb{R}^d} |\phi(\boldsymbol{x})|^2 \mathrm{d}\boldsymbol{x} = 1,\ E(\phi) < \infty\}$. The GPE (1)-(3) proves to be valid for the dipolar BEC on the mean field level [16, 35, 53], however it fails to describe the quantum fluctuation [28] of the condensate. Hence, one needs to go beyond the mean field theory and the very first step is to investigate the collective excitation so as to capture the many body effect of interatomic interactions. The collective excitation could be analyzed via elementary excitation of the system governed by GPE (1). Under proper assumption of the dipolar BEC, the elementary excitation around the mean field stationary state could be well described within the Bogoliubov theory, which resulted in the celebrated Bogoliubov-de Gennes equations (BdGEs) [8, 29, 24, 37, 41]. To date, the analysis works on the elementary excitations in BECs are mainly composed of GPE for describing the condensed part and Bogoliubov theory for describing the non-condensed part, respectively [28].

Great enthusiasm has been stimulated to investigate BdGEs in physics literature [28, 44] in the past few decades, most of which are about non-dipolar systems. Based on the low energy excitation of a dilute Boson gas in harmonic traps, Stringari [44] obtains the long wave excitation frequency of a trapped BEC in a Thomas-Fermi regime. A method to find analytical solutions of BdGEs for the low-lying collective excitation in harmonic trap potential beyond the Thomas-Fermi regime was proposed by Hu et al. [28]. Along the numerical front, there have been quite a few developments. Edwards[20, 40] applied the finite difference method and solved the sparse algebraic eigenvalue system using the ARPACK library. Danaila et al. investigated the BdGEs of a multi-component BEC with finite-element method[19]. Gao and Cai systematically studied BdGEs for the classical GPE and proposed several efficient algorithms, including the compact finite difference method, sine spectral method[24]. On the contrast, there are few theoretical studies on the excitation of dipolar BEC. For the numerical studies, there are some papers that mainly consider the lower-dimensional cases ($d = 1$ or 2). For example, Yi et al. [29] studied the low-lying collective excitation of the rotating quasi-two-dimensional system with Fourier spectral method and Ronen et al. [41, 50] developed an algorithm based on the one-dimensional discrete Hankel transform for cylindrically symmetric system. Those works are either mainly for lower dimensional cases or systems with specific symmetric structure, and they are disadvantageous in evaluating the nonlocal DDI.

Furthermore, to the best of our knowledge, there were no systematical studies on BdGEs in the context of dipolar BEC from the mathematical standpoint. Hence, it is necessary to develop mathematical theories and to construct accurate and efficient numerical methods to solve the corresponding BdGEs. To numerically investigate the elementary excitations, the main challenge lies in (i) robust solver for the eigenvalue problem, i.e. BdGEs; (ii) accurate and efficient stationary state (8) and/or ground states solver; (iii) accurate DDI fast solver that would play a decisive role in the whole numerical method, particularly in high spatial dimensions. Fortunately, the computation of nonlocal DDI has been studied quite extensively, and many effective algorithms has been proposed, such as the sine spectral method [12, 9, 10], the NonUniform Fast Fourier Transform method (NUFFT) [13, 14, 31], Gaussian-Sum Method [21], Kernel Truncation Method (KTM) [41, 42, 48] and the Anisotropic Truncated Kernel Method (ATKM) [25]. The smooth and fast-decaying density $\rho := |\psi|^2$ can be well approximated by Fourier spectral method, and it is reasonable to expect spectral accuracy with the same efficiency when computing the nonlocal interactions. In fact, all the last three methods can achieve spectral accuracy within $O(N \log N)$ operations where N is the number of unknowns. However, the prefactors in front of $O(N \log N)$ are

usually very large, hence improvement is required to achieve better efficiency, especially for problems in high space dimension. In this paper, starting from the density's Fourier spectral approximation, we will propose an even simpler method (in Section 3.2) to compute the nonlocal DDI. The proposed nonlocal solver achieves spectral accuracy with an even better complexity, i.e., a smaller prefactor in $O(N \log N)$.

As for the computation of stationary/ground states, various numerical methods have been proposed for the (non)-dipolar BEC [3, 4, 9, 10, 11, 13, 18, 30, 48, 49, 51, 52], among which the preconditioned conjugate gradient (PCG) method [4] was evidenced to be one of the most efficient solver. Recently, Zhang et al [46] incorporate the ATKM for the DDI evaluation into the PCG method to compute the stationary state of a dipolar BEC. The resulted PCG-ATKM is spectrally accurate, simple to be implemented and fast (with a $O(N \log N)$ complexity). We will apply the PCG-ATKM to precompute the stationary/ground state ϕ_s for the BdGEs. With the Fourier spectral discretization in space, the resulted discrete eigen-system, i.e. the discrete BdGEs, is densely populated which shall render prohibitively huge memory costs with explicit matrix storage. Therefore, it is necessary to provide efficient matrix-free operator-function evaluation during the iterative eigenvalue process. In this paper, we will apply the matrix-free Implicitly Restarted Arnoldi Methods (IRAM), implemented efficiently via ARPACK with reverse communication interface, to solve the resulted discrete eigenvalue/vector system. Overall, the main objectives of this paper are threefold:

1. Investigate theoretically the mathematical properties of the BdGEs, focusing on its special analytical solution pairs in different regimes.
2. Develop an efficient and accurate algorithm, i.e. SFSC, for nonlocal interactions and integrate it with matrix-free IRAM to solve the discrete BdGEs via ARPACK or its variant.
3. Apply the proposed SFSC-IRAM method to investigate the excitation spectrum and Bogoliubov amplitudes of the dipolar BEC around ground state with different parameters in two and three dimensions.

The rest of the paper is organized as follows: In Section 2, we introduce the BdGEs and derive some analytical properties. In Section 3, we present the details of the Fourier spectral method for space discretization and propose the Simple Fast Spectral Convolution method for computing the nonlocal interactions as well as the approach to compute the discrete BdGEs. Extensive numerical examples are shown in Section 4 to confirm the performance of our method, together with some applications to study the solutions to the BdGEs with different parameters in 2D and 3D. Finally, conclusions are drawn in Section 5.

2. The BdGEs and its properties.

2.1. The Bogoliubov-de Gennes equations. To characterize the elementary excitations of a dipolar BEC, the Bogoliubov theory [8, 24, 37, 41] begins with the stationary state $\phi_s(\boldsymbol{x})$ of the GPE (1), which is also the solution of the nonlinear eigenvalue problem (8) with chemical potential μ_s (9), and assumes the evolution of GPE (1) is around $\phi_s(\boldsymbol{x})$. The corresponding wave function ψ would then take the form [24, 41]

$$\psi(\boldsymbol{x},t) = e^{-i\mu_s t}\left[\phi_s(\boldsymbol{x}) + p\sum_{j=1}^{\infty}\left(u_j(\boldsymbol{x})e^{-i\omega_j t} + \bar{v}_j(\boldsymbol{x})e^{i\omega_j t}\right)\right], \ \boldsymbol{x}\in\mathbb{R}^d, t>0. \tag{11}$$

Here, $\bar{v}_j$ denotes the complex conjugate of v_j, $0 < p \ll 1$ is a small quantity used to control the population of quasiparticle excitation, $\omega_j \in \mathbb{C}$ is the frequency of the excitations to be determined and $u_j(\boldsymbol{x})$ & $v_j(\boldsymbol{x})$ are the corresponding Bogoliubov excitation modes satisfying the following normalization condition

$$\int_{\mathbb{R}^d} \left(|u_j(\boldsymbol{x})|^2 - |v_j(\boldsymbol{x})|^2\right) \mathrm{d}\boldsymbol{x} = 1, \quad j \in \mathbb{Z}^+. \tag{12}$$

Plugging (11) into (1)-(2), by collecting the linear terms in p and separating the frequency $e^{-i\omega_j t}$ and $e^{i\omega_j t}$, we obtain the following BdGEs

$$\mathcal{L}_{\mathrm{GP}} u_j + \beta|\phi_s|^2 u_j + \beta\phi_s^2\, v_j + \lambda\, U * \left(\bar{\phi}_s u_j + \phi_s v_j\right)\phi_s = \quad \omega_j\, u_j, \tag{13}$$

$$\mathcal{L}_{\mathrm{GP}} v_j + \beta\bar{\phi}_s^2 u_j + \beta|\phi_s|^2 v_j + \lambda\, U * \left(\bar{\phi}_s u_j + \phi_s v_j\right)\bar{\phi}_s = -\omega_j v_j, \tag{14}$$

with

$$\mathcal{L}_{\mathrm{GP}} := -\frac{1}{2}\nabla^2 + V(\boldsymbol{x}) + \beta|\phi_s|^2 + \lambda\Phi_s - \mu_s, \quad \Phi_s = U * |\phi_s|^2. \tag{15}$$

Under proper assumption, it has been shown that the stationary states $\phi_s(\boldsymbol{x})$ is unique up to a constant phase factor [9] and can be chosen as a real-valued function $\phi_s^R(\boldsymbol{x})$, i.e., $\phi_s(\boldsymbol{x}) = \phi_s^R(\boldsymbol{x})\, e^{i\theta}$ with $\theta \in \mathbb{R}$. It is easy to check that the different choice of ϕ_s with different phase factor θ only resulted in different Bogoliubov amplitude functions with a phase factor, i.e., if (ω_j, u_j, v_j) solves BdGEs (13)-(14) with ϕ_s, then $(\omega_j, e^{i\theta}\, u_j, e^{-i\theta}\, v_j)$ solves BdGEs (13)-(14) with $e^{i\theta}\phi_s$. Thus, it suffices to consider the real-valued stationary states case and we shall assume $\phi(\boldsymbol{x}) \in \mathbb{R}$ throughout this paper. To simplify the presentation, hereafter we remove all subscripts for u_j, v_j & w_j and write them indiscriminately as u, v & w, respectively. Denote operators

$$\begin{aligned} \mathcal{L}_{11} &= \mathcal{L}_{\mathrm{GP}} + \beta\,|\phi_s|^2 + \lambda\,\widehat{\chi}_1, \qquad \mathcal{L}_{12} = \beta\,\phi_s^2 + \lambda\,\widehat{\chi}_2, \\ \mathcal{L}_{22} &= -\mathcal{L}_{\mathrm{GP}} - \beta\,|\phi_s|^2 - \lambda\,\widehat{\chi}_1^*, \qquad \mathcal{L}_{21} = -\beta\bar{\phi}_s^2 - \lambda\,\widehat{\chi}_2^*, \end{aligned} \tag{16}$$

with nonlocal actions $\widehat{\chi}_j$ & $\widehat{\chi}_j^*$ $(j = 1, 2)$ defining as

$$\begin{aligned} \widehat{\chi}_1(\xi) &:= \phi_s\left[U * (\bar{\phi}_s\xi)\right], \qquad \widehat{\chi}_2(\xi) := \phi_s\left[U * (\phi_s\xi)\right], \\ \widehat{\chi}_1^*(\xi) &:= \bar{\phi}_s\left[U * (\phi_s\xi)\right], \qquad \widehat{\chi}_2^*(\xi) := \bar{\phi}_s\left[U * (\bar{\phi}_s\xi)\right], \end{aligned} \tag{17}$$

the BdGEs (13)-(14) with constraint (12) could be equivalently recasted as

$$\begin{pmatrix} \mathcal{L}_{11} & \mathcal{L}_{12} \\ \mathcal{L}_{21} & \mathcal{L}_{22} \end{pmatrix} \begin{pmatrix} u \\ v \end{pmatrix} = \omega \begin{pmatrix} u \\ v \end{pmatrix}, \tag{18}$$

with constraint

$$\int_{\mathbb{R}^d} \left(|u(\boldsymbol{x})|^2 - |v(\boldsymbol{x})|^2\right) d\boldsymbol{x} = 1. \tag{19}$$

Specially, for the real-valued stationary state ϕ_s, all the nonlocal operators are identical, i.e., $\widehat{\chi}_1 \equiv \widehat{\chi}_2 \equiv \widehat{\chi}_1^* \equiv \widehat{\chi}_2^*$. By applying a change of variables

$$u(\boldsymbol{x}) = f(\boldsymbol{x}) + g(\boldsymbol{x}), \qquad v(\boldsymbol{x}) = f(\boldsymbol{x}) - g(\boldsymbol{x}), \tag{20}$$

the BdGEs (18) could be simplified as

$$H_+ f(\boldsymbol{x}) = \omega g(\boldsymbol{x}), \qquad H_- g(\boldsymbol{x}) = \omega f(\boldsymbol{x}), \quad \Re\left(\int_{\mathbb{R}^d} (f(\boldsymbol{x})\,\bar{g}(\boldsymbol{x}))\, d\boldsymbol{x}\right) = \frac{1}{4}, \tag{21}$$

which immediately leads to a decoupled linear eigen-system

$$H_- H_+ f(\boldsymbol{x}) = \omega^2 f(\boldsymbol{x}), \qquad H_+ H_- g(\boldsymbol{x}) = \omega^2 g(\boldsymbol{x}). \tag{22}$$

Here, $\Re(\alpha)$ denotes the real part of α and $H_+ := \mathcal{L}_{\rm GP} + 2\beta|\phi_s|^2 + 2\lambda\hat{\chi}_1$, $H_- := \mathcal{L}_{\rm GP}$. One could solve the above decoupled unconstrained eigenvalue problems (22) instead of the coupled constrained system (18), which is common in physics community[41]. Alternatively, we can directly treat (18) as a linear response problem and solve it by the locally optimal block preconditioned 4D conjugate gradient algorithm or its variants [6, 7].

Due to the nonlocal character of DDI, the BdGEs are very difficult for both analytical and numerical analysis. Only for several low energy excitation modes, it is possible to obtain some analytic results by using a Gaussian variational ansatz [35] or the Thomas–Fermi approximation [28]. Here we investigate the typical harmonic trapping potential case (4), and derive some analytical properties of BdGEs, which could serve as benchmarks for testing numerical methods.

2.2. Analytical properties of BdGEs. For general potential $V(\boldsymbol{x})$, we have the following results.

LEMMA 1. *If $\{u, v, \omega\}$ ($\omega \in \mathbb{C}$) is a solution pair to the BdGEs (18), then $\{\bar{v}, \bar{u}, -\bar{\omega}\}$ is also a solution to the BdGEs(18) and*

$$(\omega - \bar{\omega}) \int_{\mathbb{R}^d} (|u(\boldsymbol{x})|^2 - |v(\boldsymbol{x})|^2)\, d\boldsymbol{x} = 0. \tag{23}$$

Furthermore, if $u(\boldsymbol{x})$, $v(\boldsymbol{x})$ satisfy the normalization constraint (19), i.e., the elementary excitations, the eigen-frequency ω then is real.

Proof. Take conjugate of (13)-(14) on both sides, we have

$$\begin{aligned}
&\mathcal{L}_{\rm GP}\bar{u} + \beta(\bar{\phi}_s)^2\bar{v} + \beta|\phi_s|^2\bar{u} + \lambda U * (\bar{\phi}_s\bar{v} + \phi_s\bar{u})\bar{\phi}_s = \ \bar{\omega}\bar{u},\\
&\mathcal{L}_{\rm GP}\bar{v} + \beta|\phi_s|^2\bar{v} \ + \beta\phi_s^2\bar{u} \ \ + \ \lambda U * (\bar{\phi}_s\bar{v} + \phi_s\bar{u})\phi_s = -\bar{\omega}\bar{v},
\end{aligned}$$

which immediately implies that $\{\bar{v}, \bar{u}, -\bar{\omega}\}$ is also a solution. Multiplying (13)-(14) respectively by $\bar{u}$ and $\bar{v}$, integrating over $\mathbb{R}^d$ and combining the resulted equations, we obtain

$$\begin{aligned}
&\omega \int_{\mathbb{R}^d} (|u(\boldsymbol{x})|^2 - |v(\boldsymbol{x})|^2) d\boldsymbol{x}\\
&\quad = \int_{\mathbb{R}^d} \Big\{ \frac{1}{2}\left(|\nabla u(\boldsymbol{x})|^2 + |\nabla v(\boldsymbol{x})|^2\right) + (V + 2\beta|\phi_s|^2 + \lambda\Phi_s - \mu_s)(|u(\boldsymbol{x})|^2 + |v(\boldsymbol{x})|^2)\\
&\qquad + \beta\Big(\phi_s^2\bar{u}v + \bar{\phi}_s^2 u\bar{v}\Big) + \lambda\Big[\bar{u}\hat{\chi}_1(u) + \bar{v}\hat{\chi}_1^*(v) + \bar{u}\hat{\chi}_2(v) + \bar{v}\hat{\chi}_2^*(u)\Big]\Big\} d\boldsymbol{x}.
\end{aligned} \tag{24}$$

□

It is easy to check that the RHS of (24) is real and hence substitute equation (24) from its conjugate, we arrive at the identity (23).

REMARK 1. *From this lemma, we note that under the normalization constrain (19) only the real eigenvalues for BdGEs are relevant for the elementary excitations. Complex eigenvalues, which play a crucial rule in determining the dynamical stability of stationary states, may occur for BdGEs (18) only if $\|u\| = \|v\|$. Now that we focus on the elementary excitation, i.e., BdGEs (18) with constrain (19), we reasonably assume ω is real throughout this paper and leave the study of complex eigenvalues of BdGEs as future work.*

For harmonic potential $V(\boldsymbol{x}) = \frac{1}{2}\sum_\alpha \gamma_\alpha^2 \alpha^2$ with spatial variables $\alpha = x, y$ in 2D and $\alpha = x, y, z$ in 3D, we have the following results for the corresponding Bogoliubov excitations.

LEMMA 2. *Let ϕ_s be the real-valued stationary state of GPE (1), then we have the following solution pair to the BdGEs (18) with constrain (19):*

$$\{u_\alpha, v_\alpha, \omega_\alpha\} =: \left\{ \frac{1}{\sqrt{2}}\left(\gamma_\alpha^{-1/2}\partial_\alpha\phi_s - \gamma_\alpha^{1/2}\alpha\phi_s\right),\ \frac{1}{\sqrt{2}}\left(\gamma_\alpha^{-1/2}\partial_\alpha\phi_s + \gamma_\alpha^{1/2}\alpha\phi_s\right),\ \gamma_\alpha \right\},$$

with $\alpha = x, y$ in 2D and $\alpha = x, y, z$ in 3D.

Proof. Notice that stationary state ϕ_s satisfies the Euler-Lagrange equation (8), differentiating (8) with respect to variable x, we have

$$H_+(\partial_x\phi_s) = (-\frac{1}{2}\nabla^2 + V + 3\beta|\phi_s|^2 + \lambda\Phi_s + 2\lambda\hat{\chi}_1 - \mu_s)(\partial_x\phi_s) = \gamma_x(-\gamma_x x\phi_s).$$

Apply H_- on $-\gamma_x x$ and combine Eqn. (8), we have

$$H_-(-\gamma_x x\phi_s) = (-\frac{1}{2}\nabla^2 + V + \beta|\phi_s|^2 + \lambda\Phi_s - \mu_s)(-\gamma_x x\phi_s) = \gamma_x(\partial_x\phi_s).$$

Therefore, it is clear that $(\partial_x\phi_s, -\gamma_x x\phi_s)$ solves Eqn.(21) with $\omega = \gamma_x$. Noticing $-\int_{\mathbb{R}^2}\gamma_x x\phi_s\partial_x\phi_s \mathrm{d}x\mathrm{d}y = \frac{\gamma_x}{2}$, we conclude that $(f, g) = (\frac{1}{\sqrt{2}}\gamma_x^{-\frac{1}{2}}\partial_x\phi_s, -\frac{1}{\sqrt{2}}\gamma_x^{\frac{1}{2}}x\phi_s)$ solves (22) under the normalization constraint for $\omega = \gamma_x$. Using (20), we dervie the following analytic solution

$$\omega_x = \gamma_x, \quad u_x = \frac{1}{\sqrt{2}}\left(\gamma_x^{-\frac{1}{2}}\partial_x\phi_s - \gamma_x^{\frac{1}{2}}x\phi_s\right), \quad v_x = \frac{1}{\sqrt{2}}\left(\gamma_x^{-\frac{1}{2}}\partial_x\phi_s + \gamma_x^{\frac{1}{2}}x\phi_s\right).$$

The conclusion holds true for $\alpha = y, z$ following similar argument, and we omit the proof for brevity. ∎

In addition, in the Thomas-Fermi (TF) regime, i.e. $\beta \gg 1$, for dipolar BECs with dipoles lying along the z-axis, i.e., $\boldsymbol{n} = (0, 0, 1)^T$ and trapped by a cylindrically symmetric harmonic trapping potential $V(\boldsymbol{x})$, i.e., $\gamma_x = \gamma_y$ in (4), we have the following results for the ground state profile $\phi_g(\boldsymbol{x})$ and the corresponding Bogoliubov excitations.

LEMMA 3. *The ground state profile $\phi_g(\boldsymbol{x})$ of GPE (10) could be well approximated by the TF density $\phi_g^{\mathrm{TF}}(\boldsymbol{x})$ with chemical potential μ_g^{TF} [22]:*

$$\phi_g(\boldsymbol{x}) \approx \phi_g^{\mathrm{TF}}(\boldsymbol{x}) := \sqrt{\frac{15}{8\pi R^2 R_z}\left(1 - \frac{x^2}{R^2} - \frac{y^2}{R^2} - \frac{z^2}{R_z^2}\right)_+}.$$

Here, $\mu_g^{\mathrm{TF}} = \frac{15\,(\beta - \lambda\,\eta(\kappa))}{8\pi R^2 R_z}$ is the chemical potential, $f_+(\boldsymbol{x}) := \max\{0, f(\boldsymbol{x})\}$ and

$$\eta(\kappa) := \begin{cases} \dfrac{1+2\kappa^2}{1-\kappa^2} - \dfrac{3\kappa^2\mathrm{arctanh}(\sqrt{1-\kappa^2})}{(1-\kappa^2)^{3/2}}, & \kappa \le 1, \\ \dfrac{1+2\kappa^2}{\kappa^2-1} - \dfrac{3\kappa^2\arctan(\sqrt{\kappa^2-1})}{(\kappa^2-1)^{3/2}}, & \kappa > 1, \end{cases}$$

where the ratio $\kappa := R/R_z$ is determined by the following transcendental equation

$$\frac{3\lambda\kappa^2}{\beta}\left[\left(\frac{\gamma_z^2}{2\gamma_x^2}+1\right)\frac{\eta(\kappa)}{1-\kappa^2}-1\right]+\left(\frac{\lambda}{\beta}-1\right)\left(\kappa^2-\frac{\gamma_z^2}{\gamma_x^2}\right)=0. \tag{25}$$

The radii R is given explicitly as

$$R=\left[\frac{15\kappa}{4\pi\gamma_x^2}\beta\left(1+\frac{\lambda}{\beta}\left(\frac{3\kappa^2\eta(\kappa)}{2(1-\kappa^2)}-1\right)\right)\right]^{\frac{1}{5}}. \tag{26}$$

Moreover, as $\beta\to\infty$, we have the asymptotic results

$$R=\mathcal{O}(\beta^{1/5}),\qquad R_z=\mathcal{O}(\beta^{1/5}),\qquad \mu_g^{\mathrm{TF}}=\mathcal{O}(\beta^{2/5}).$$

LEMMA 4. *Under the same conditions of Lemma 3, the Bogoliubov eigenvalues associated with(13)-(14), denoted by ω_β, is well approximated by ω_∞ as $\beta\to\infty$. The limit eigenvalue ω_∞ satisfies*

$$-\left(1-\frac{1}{2}(\gamma_x^2x^2+\gamma_x^2y^2+\gamma_z^2z^2)\right)\nabla^2q+(\gamma_x^2x\partial_x+\gamma_y^2y\partial_y+\gamma_z^2z\partial_z)q=(\omega_\infty)^2q(\boldsymbol{x}),$$

for $\boldsymbol{x}\in D_\infty:=\left\{\boldsymbol{x}\in\mathbb{R}^3\middle|1-\frac{1}{2}(\gamma_x^2x^2+\gamma_x^2y^2+\gamma_z^2z^2)\geq 0\right\}$. Especially, for a special isotropic harmonic trap, i.e. $\gamma_x=\gamma_y=\gamma_z=\sqrt{2}$, we have the explicit eigenvalues

$$\omega_\infty^{l,k}=\sqrt{2}\sqrt{l+3k+2kl+2k^2},\qquad l\geq 0,\quad k\geq 0.$$

Proof. To estimate the asymptotics of ω_β for large β, we first introduce the rescaling $\widetilde{\boldsymbol{x}}=\boldsymbol{x}/\sqrt{\mu_g}$ and $\phi_g(\boldsymbol{x})=\sqrt{\frac{\mu_g}{\beta}}\widetilde{\phi}_g(\widetilde{\boldsymbol{x}})$, then we obtain the following formula

$$\begin{aligned}&\Phi_g(\boldsymbol{x})=\frac{\mu_g}{\beta}\widetilde{\Phi}_g(\widetilde{\boldsymbol{x}}),&&\widetilde{\Phi}_g(\widetilde{\boldsymbol{x}}):=\left(U*|\widetilde{\phi_g}|^2\right)(\widetilde{\boldsymbol{x}}),\\&\left[\hat{\chi}(f)\right](\boldsymbol{x})=\frac{\mu_g}{\beta}\left[\widehat{\widetilde{\chi}}(\widetilde{f})\right](\widetilde{\boldsymbol{x}}),&&f(\boldsymbol{x})=\widetilde{f}(\widetilde{\boldsymbol{x}}).\end{aligned}$$

The second BdG equation (22), i.e. $H_+H_-g=\omega^2g$, is now rescaled as $\widetilde{H}_+\widetilde{H}_-\widetilde{g}=\frac{\omega^2}{\mu_g^2}\widetilde{g}$ with

$$\widetilde{H}_+=-\frac{1}{2\mu_g^2}\widetilde{\nabla}^2+\widetilde{V}(\widetilde{\boldsymbol{x}})+3|\widetilde{\phi}_g|^2+\frac{\lambda}{\beta}\widetilde{\Phi}_g+2\frac{\lambda}{\beta}\widetilde{\chi}-1,\qquad \widetilde{H}_-=\widetilde{H}_+-2|\widetilde{\phi}_g|^2-2\frac{\lambda}{\beta}\widetilde{\chi}, \tag{27}$$

and $\widetilde{\nabla}^2=\frac{\partial^2}{\partial\widetilde{x}^2}+\frac{\partial^2}{\partial\widetilde{y}^2}+\frac{\partial^2}{\partial\widetilde{z}^2},\widetilde{V}(\widetilde{\boldsymbol{x}})=\frac{1}{2}(\gamma_x^2\widetilde{x}^2+\gamma_x^2\widetilde{y}^2+\gamma_z^2\widetilde{z}^2)$. The eigenvalue problem (8) is then rescaled as

$$\left[-\frac{1}{2}\frac{1}{\mu_g^2}\widetilde{\nabla}^2+\widetilde{V}(\widetilde{\boldsymbol{x}})+|\widetilde{\phi}_g|^2+\frac{\lambda}{\beta}\widetilde{\Phi}_g\right]\widetilde{\phi}_g=\widetilde{\phi}_g. \tag{28}$$

Combing (27)-(28), we have

$$\left[-\frac{1}{2\mu_g^2}\widetilde{\nabla}^2+\widetilde{V}(\widetilde{\boldsymbol{x}})+3|\widetilde{\phi}_g|^2+\frac{\lambda}{\beta}\widetilde{\Phi}_g+2\frac{\lambda}{\beta}\widetilde{\chi}-1\right]\left[-\frac{1}{2\mu_g^2}\widetilde{\nabla}^2+\frac{1}{2\mu_g^2}\frac{1}{\widetilde{\phi}_g}\widetilde{\nabla}^2\widetilde{\phi}_g\right]\widetilde{g}=\frac{\omega^2}{\mu_g^2}\widetilde{g}.$$

In Thomas-Fermi regime ($\beta \gg 1$), the rescaled $\widetilde{\phi}_g^{\rm TF}$ converges to $\widetilde{\phi}_g^{\infty}(\widetilde{\boldsymbol{x}}) = \left(1-\frac{1}{2}(\gamma_x^2\widetilde{x}^2+\gamma_y^2\widetilde{y}^2+\gamma_z^2\widetilde{z}^2)\right)_+^{\frac{1}{2}}$ as $\beta\to\infty$. In the above equation, by substituting $\widetilde{\phi}_g^{\rm TF}, \widetilde{\mu}_g^{\rm TF}$ for the ground state $\widetilde{\phi}_g$ and the chemical potential μ_g respectively, we obtain the following eigenvalue problem

$$\left[\frac{-1}{2(\mu_g^{\rm TF})^2}\widetilde{\nabla}^2+\widetilde{V}(\widetilde{\boldsymbol{x}})+3|\widetilde{\phi}_g^{\rm TF}|^2-1\right]\left[-\frac{1}{2(\mu_g^{\rm TF})^2}\widetilde{\nabla}^2+\frac{1}{2(\mu_g^{\rm TF})^2}\frac{1}{\widetilde{\phi}_g^{\rm TF}}\widetilde{\nabla}^2\widetilde{\phi}_g^{\rm TF}\right]\widetilde{g}\approx\frac{\omega^2}{(\mu_g^{\rm TF})^2}\widetilde{g}.$$

When $\beta\to\infty$, by plugging in the limit function $\widetilde{\phi}_g^{\infty}$ and dropping higher order term of $1/\mu_g^{\rm TF}$, we derive the limit eigenvalue problem for $q=\widetilde{g}/\widetilde{\phi}_g^{\rm TF}$ as follows

$$(29)-\left(1-\frac{1}{2}(\gamma_x^2\widetilde{x}^2+\gamma_x^2\widetilde{y}^2+\gamma_z^2\widetilde{z}^2)\right)\widetilde{\nabla}^2 q+(\gamma_x^2\widetilde{x}\partial_{\widetilde{x}}+\gamma_y^2\widetilde{y}\partial_{\widetilde{y}}+\gamma_z^2\widetilde{z}\partial_{\widetilde{z}})q=\omega_\infty^2 q(\widetilde{\boldsymbol{x}}).$$

Especially, when $\gamma_x=\gamma_y=\gamma_z=\sqrt{2}$, $q(\boldsymbol{x})$ is spherically symmetric, hence Eqn. (29) could be solved explicitly in a similar way as shown in [34]. ∎

3. Numerical method. In this section, we will propose an efficient and spectral-accurate numerical methods to solve the BdGEs (18) with constraint (19). Due to the external trapping potential $V(\boldsymbol{x})$, the wave function $\psi(\boldsymbol{x})$ and the ground/stationary states $\phi_s(\boldsymbol{x})$ to the GPE (1)-(3), as well as the eigenfunctions $(u(\boldsymbol{x}), v(\boldsymbol{x}))$ to the BdGEs (18)-(19) are all smooth and fast-decaying. Therefore, it is reasonable to truncate the whole space $\mathbb{R}^d$ into a bounded domain $\mathcal{D}\subset\mathbb{R}^d$ with periodic boundary conditions such that the truncation error is negligible. To numerically solve the BdGEs, high spatial resolution schemes are usually preferred. In terms of accuracy, simplicity and efficiency, the Fourier pseudo-spectral (FS) discretization [9, 10, 11] is one of the most optimal candidate. However, due to the polynomially decaying properties (at the far field $|\boldsymbol{x}|\to\infty$) of the convolution-type nonlocal potentials Φ_s (15) and the nonlocal interaction $\chi_j(\xi)$ (17) , the FS scheme could not be directly applied. Indeed, it is the most challenging job to compute such nonlocal interactions with spectral accuracy as efficiently as possible. Alternative spectral-accurate solvers, such as the KTM [48] and NUFFT method[13, 31], usually require prohibitively huge memory and/or expensive computational cost, thus bottleneck the overall efficiency. In this section, we will propose a spectral-accurate solver to evaluate such nonlocal interactions via direct FS discretizations with minimal storage and optimal efficiency, then the full FS scheme for the BdGEs (18) achieves both optimal accuracy and efficiency.

3.1. Space discretization and eigen-system solver. We first introduce the Fourier pseudospectral scheme [9, 10, 11] to discretize the BdGEs (18). Provided that the stationary states ϕ_s is computed accurately by the PCG method[4, 5, 46], and the DDI potential Φ_s can be easily evaluated by the SFSC method, which is to be introduced in next section. For simplicity, we only present the scheme for the 2D case. We choose the computation domain $\mathcal{D}$ as a square for simplicity and denote it by $\mathcal{D}_L := [-L,L]\times[-L,L]$. Let N and M be two positive even integers. Choose $h_x=\frac{2L}{N}$ and $h_y=\frac{2L}{M}$ as the mesh size in x- and y- directions, respectively. Define

the indices and grids points sets as

$$\mathcal{I}_{NM} = \Big\{(n,m) \in \mathbb{N}^2 \,|\, 0 \le n \le N-1,\ 0 \le m \le M-1\Big\},$$
$$\widetilde{\mathcal{I}}_{NM} = \Big\{(\ell,k) \in \mathbb{Z}^2 \,|\, -N/2 \le \ell \le N/2-1,\ -M/2 \le k \le M/2-1\Big\},$$
$$\mathcal{T}_{\boldsymbol{x}} = \Big\{(x_n,\, y_m) =: (-L + n\,h_x,\ -L + m\,h_y), \quad (n,m) \in \mathcal{I}_{NM}\Big\},$$

and introduce the following functions

$$W_{\ell k}(x,y) = e^{i\mu_\ell^x (x+L)} e^{i\mu_k^y (y+L)}, \quad (\ell,k) \in \widetilde{\mathcal{I}}_{NM}, \tag{30}$$

with $\mu_\ell^x = \frac{2\pi\ell}{2L}$, $\mu_k^y = \frac{2\pi k}{2L}$. Moreover, we define $P_{nm} =: P(x_n, y_m)$ ($P = u, v, \phi_s, \Phi_s$, etc) as the value of an abstract function $P(x,y)$ at grid $(x_n, y_m) \in \mathcal{T}_{\boldsymbol{x}}$ and $\boldsymbol{P}$ as the vector with components $\{P_{nm}\}$. The Fourier pseudo-spectral approximation of P (denoted by $\widetilde{P}$) and $\nabla^2 P$ reads as

$$P(x,y) \approx \widetilde{P}(x,y) := \sum_{\ell=-N/2}^{N/2-1} \sum_{k=-M/2}^{M/2-1} \widehat{\boldsymbol{P}}_{\ell k}\, W_{\ell k}(x,y), \tag{31}$$

$$(\nabla^2 P) \approx (\nabla^2 \widetilde{P}) := \sum_{\ell=-N/2}^{N/2-1} \sum_{k=-M/2}^{M/2-1} -\Big((\mu_\ell^x)^2 + (\mu_k^y)^2\Big)\, \widehat{\boldsymbol{P}}_{\ell k}\, W_{\ell k}(x,y), \tag{32}$$

where $\widehat{\boldsymbol{P}} \in \mathbb{C}^{NM}$, the discrete Fourier transform coefficient of $\boldsymbol{P}$, is computed as

$$\widehat{\boldsymbol{P}}_{\ell k} = \frac{1}{NM} \sum_{n=0}^{N-1} \sum_{m=0}^{M-1} P_{nm}\, \overline{W}_{\ell k}(x_n, y_m), \qquad (\ell,k) \in \widetilde{\mathcal{I}}_{NM}. \tag{33}$$

The nonlocal operators $\widehat{\chi}_j$ & $\widehat{\chi}_j^*$ ($j = 1, 2$) are approximated respectively as

$$(\widehat{\chi}_j P)(x,y) \approx (\widehat{\chi}_j \widetilde{P})(x,y), \qquad (\widehat{\chi}_j^* P)(x,y) \approx (\widehat{\chi}_j^* \widetilde{P})(x,y), \qquad (x,y) \in \mathcal{D},$$

and the operators $\mathcal{L}_{\rm GP}$ and $\mathcal{L}_{ij}$ ($i, j = 1, 2$) in (16) are then discretized at $\boldsymbol{x}_{nm} := (x_n, y_m) \in \mathcal{T}_{\boldsymbol{x}}$ as follows

$$(\mathcal{L}_{\rm GP} P)(\boldsymbol{x}_{nm}) \approx -\frac{1}{2}(\nabla^2 \widetilde{P})(\boldsymbol{x}_{nm}) + (V_{nm} + \beta|(\phi_s)_{nm}|^2 + \lambda(\Phi_s)_{nm} - \mu_s)\widetilde{P}(\boldsymbol{x}_{nm}),$$
$$(\mathcal{L}_{ij} P)(\boldsymbol{x}_{nm}) \approx (\mathcal{L}_{ij} \widetilde{P})(\boldsymbol{x}_{nm}) := (\mathbf{L}_{ij}\mathbf{P})_{nm}.$$

The BdGEs (18) with constraint (19) then could be discretized into the following linear algebraic system:

$$\begin{pmatrix} \mathbf{L}_{11} & \mathbf{L}_{12} \\ \mathbf{L}_{21} & \mathbf{L}_{22} \end{pmatrix} \begin{pmatrix} \boldsymbol{u} \\ \boldsymbol{v} \end{pmatrix} = \omega \begin{pmatrix} \boldsymbol{u} \\ \boldsymbol{v} \end{pmatrix}, \qquad h_x h_y \Big(\|\boldsymbol{u}\|^2 - \|\boldsymbol{v}\|^2\Big) = 1, \tag{34}$$

with $\|\cdot\|$ being the standard l^2 norm.

Then we describe the approach to solve the discrete BdGEs (34) briefly. First, the stationary states ϕ_s and chemical potential μ_s (34) are precomputed via the preconditioned conjugated gradient method [4, 46] in a large enough domain with small enough mesh size such that the errors coming from this evaluation are negligible.

The values of ϕ_s on grid points $\mathcal{T}_{\boldsymbol{x}}$ are interpolated by the Fourier spectral method. The involved nonlocal potentials/operators, such as Φ_s and $\widehat{\chi}_j (j = 1, 2)$, are evaluated by the nonlocal solver to be introduced in next section. Secondly, we solve the linear eigenvalue/vector problem (34). In practice, the Implicitly Restarted Arnoldi Methods (IRAM) [43] is adapted to simultaneously compute the first few smallest positive eigenvalues ω and their associated eigenvectors $(\boldsymbol{u}, \boldsymbol{v})$, followed by a rescaling in order to meet the normalization constraint. One important note is that the matrix of (34) is non-symmetric and dense, therefore explicit matrix representation requires expensive memory storage. This would notably bottleneck the efficiency if one directly applies the IRAM, especially for the 3D problems. Hence, it is essentially and necessary to utilise matrix-free version of the IRAM, which could be well resolved by coding with the well-known ARPACK [47] library. In such case, all that one needs is to provide the matrix-vector product (operator-function action on the continuous level), that is, to compute $\mathbf{L}_{i1}\boldsymbol{u}^p + \mathbf{L}_{i2}\boldsymbol{v}^p$ where vector $\boldsymbol{u}^p, \boldsymbol{v}^p \in \mathbb{C}^{NM}$ are updated iteratively.

The discrete Fourier transform and its inverse (31)-(33) could be computed efficiently via the FFT & iFFT within $O(NM \log(NM))$ operations. All the other operators in $\mathcal{L}_{ij}$ except the nonlocal interaction $\widehat{\chi}_j$ are in fact multiplication operators in the physical space, thus their operations on $\boldsymbol{u}$ & $\boldsymbol{v}$ could be easily accessed by pointwise function multiplication. The nonlocal interaction consists of convolution and function multiplication, therefore, it is not diagonalizable in either phase or physical space, which bottlenecks the overall efficiency as well as the accuracy. Therefore, the efficient and accurate evaluation of the nonlocal potentials is of essential importance in solving the BdGEs. In next subsection, we shall propose a *Simple Fast Spectral Convolution* (SFSC) algorithm, which could optimally evaluate such nonlocal interactions with spectral accuracy within $O(NM \log(NM))$ operations.

3.2. Simple Fast Spectral Convolution method for the nonlocal interactions. It is clear that all the nonlocal interactions are composed of convolution and function multiplication. The multiplication with the stationary state ϕ_s (or its conjugate) is quite straightforward, thus we concentrate on the convolution in this subsection. Without loss of generality, we consider $\varphi := U * (\phi_s f)$ with f being smooth and fast-decaying on the same computational domain $\mathcal{D}$. The kernel U is singular at the origin and decays polynomially at the far field, and the density $\rho := \phi_s f$ is smooth and fast-decaying too. The convolution evaluation is quite challenging in terms of both accuracy and efficiency, even though it can be transformed to Coulomb potential ($U(\boldsymbol{x}) = 1/(2\pi|\boldsymbol{x}|)$). For example, the convolution can be equivalently rewritten as

$$\varphi = \left(\frac{1}{2\pi|\boldsymbol{x}|}\right) * \left(-\frac{3}{2}(\partial_{n_\perp n_\perp} - n_3^2\nabla_\perp^2)\rho\right) := \left(\frac{1}{2\pi|\boldsymbol{x}|}\right) * \widetilde{\rho}, \tag{35}$$

where $\widetilde{\rho}$ is the effective DDI-density for the 2D Coulomb potential. The 3D convolution can also be transformed to Coulomb potential with similar kernel $U(\boldsymbol{x}) = 1/(4\pi|\boldsymbol{x}|)$, and we omit details for brevity.

To simplify the presentation, we assume the computational domain $\mathcal{D} = \mathcal{D}_L := \prod_{j=1}^{d}[-L, L]$ is a cube centered at the origin of length $2L$ in each spatial direction. Existing convolution solvers either requires extra zero-padding [48] or performs inefficiently in higher spatial dimensions [31, 13]. We now propose an efficient approach which requires optimal two-fold zero-padding and is easily implemented with FFT/iFFT. To be exact, we take 2D case as an example as follows.

For simplicity's sake, we replace $\widetilde{\rho}$ by ρ and assume further that the density is compactly supported (numerically) in $\mathcal{D}_L$. To compute the interaction at $\boldsymbol{x} \in \mathcal{D}_L$, we

have

$$\varphi(\boldsymbol{x}) = \int_{\mathbb{R}^2} U(\boldsymbol{y})\rho(\boldsymbol{x}-\boldsymbol{y})\mathrm{d}\boldsymbol{y}, \quad \boldsymbol{x} \in \mathcal{D}_L, \tag{36}$$

$$= \int_{\boldsymbol{x}+\mathcal{D}_L} U(\boldsymbol{y})\rho(\boldsymbol{x}-\boldsymbol{y})\mathrm{d}\boldsymbol{y} = \int_{\mathcal{D}_{2L}} U(\boldsymbol{y})\rho(\boldsymbol{x}-\boldsymbol{y})\mathrm{d}\boldsymbol{y}. \tag{37}$$

For $\boldsymbol{x} \in \mathcal{D}_L$, the whole space domain $\mathbb{R}^2$ is reduced to $\boldsymbol{x}+\mathcal{D}_L$ because $\rho(\boldsymbol{x}-\boldsymbol{y}) = 0,\ \forall\ \boldsymbol{y} \notin \boldsymbol{x}+\mathcal{D}_L$, and the third equation holds true as the density is compactly supported (numerically) in $\mathcal{D}_L$. Therefore, we have $\boldsymbol{x}-\boldsymbol{y} \in \mathcal{D}_{3L}$ for $\forall\ \boldsymbol{x} \in \mathcal{D}_L,\ \boldsymbol{y} \in \mathcal{D}_{2L}$. Then we need to approximate the density ρ on $\mathcal{D}_{3L}$. However, with careful investigation on the periodicity of Fourier basis, it suffices to approximate ρ on a two-fold domain $\mathcal{D}_{2L}$, and we refer to [21] for details. After a twofold zero-padding of the density ρ, we obtain the Fourier series approximation on $\mathcal{D}_{2L}$ as follows

$$\rho(\boldsymbol{z}) \approx \sum_{p=-N}^{N-1}\sum_{q=-M}^{M-1} \widehat{\rho}_{pq}\ \ e^{i\widetilde{\mu}_p^x(x+2L)}e^{i\widetilde{\mu}_q^y(y+2L)}, \quad \boldsymbol{z} := (x,y) \in \mathcal{D}_{2L}, \tag{38}$$

with $\widetilde{\mu}_p^x = \pi p/(2L), \widetilde{\mu}_q^y = \pi q/(2L)$ and $\widehat{\rho}_{pq}$ is the discrete Fourier transform. Plugging (38) into (37) and substituting $\boldsymbol{x}-\boldsymbol{y}$ for $\boldsymbol{z}$, we have

$$\varphi(\boldsymbol{x}) \approx \sum_{p=-N}^{N-1}\sum_{q=-M}^{M-1} \widehat{\rho}_{pq}\ \widehat{U}_{pq}\ \ e^{i\widetilde{\mu}_p^x(x+2L)}e^{i\widetilde{\mu}_q^y(y+2L)}, \qquad \boldsymbol{x} \in \mathcal{D}_L, \tag{39}$$

where $\widehat{U}_{pq} =: \widehat{U}(\widetilde{\mu}_p^x, \widetilde{\mu}_q^y)$ is the Fourier transform of U on bounded domain $\mathcal{D}_{2L}$, which is given explicitly as follows

$$\widehat{U}_{pq} = \int_{\mathcal{D}_{2L}} U(\boldsymbol{x})\ e^{-i\widetilde{\mu}_p^x x}e^{-i\widetilde{\mu}_q^y y}\mathrm{d}\boldsymbol{x} = (2L)\int_{\mathcal{D}_1} U(\boldsymbol{x})\ e^{-i\pi p x}e^{-i\pi q y}\mathrm{d}\boldsymbol{x}. \tag{40}$$

The last equation holds with a change of variables $\boldsymbol{x} = 2L\widetilde{\boldsymbol{x}}$ for the Coulomb potential. The Fourier transform $\widehat{U}_{pq}$ can be reduced to a singular Fourier integral on standard domain $\mathcal{D}_1 = [-1,1]^2$, and can be pre-computed very accurately up to machine precision via some high-precision library such as the Advanpix toolbox [1]. If $\widehat{U}_{pq}$ is to be computed on-the-fly, we recommend the Gaussian-Summation acceleration techniques [25]. Once (40) is available, the Coulomb potential on $\mathcal{T}_{\boldsymbol{x}}$ can be computed with one pair FFT/iFFT and one function multiplication of size $4NM$, and the overall cost is $O(4NM + 4NM\log(4NM))$. Note that the potential φ on mesh $\mathcal{T}_{\boldsymbol{x}}$, which is a uniform partition of $\mathcal{D}_L$, is part of the inverse FFT (on a twofold zero-padded mesh), therefore, no interpolation is ever needed at this step. The efficiency is almost optimal compared with existing methods, and the accuracy achieved is close to machine precision as expected.

To summarize, the nonlocal interaction $\widehat{\chi}_j(f)$ ($\widehat{\chi}_j^*(f)$) can be computed efficiently in two steps: (i) compute the convolution with density $\phi_s f$ ($\bar{\phi}_s f$), (ii) multiply the interaction φ and the ground state ϕ_s ($\bar{\phi}_s$). We present a detailed step-by-step algorithm using $\widehat{\chi}_1(f)$ as an example, and adaptation to $\widehat{\chi}_2(f)$ and $\widehat{\chi}_j^*(f)$ are straightforward. The algorithm to compute the nonlocal interaction is summarized in Alg. 1.

To show the accuracy and efficiency, we carry out the following example. For simplicity, we only evaluate nonlocal interaction $\chi_1(f)$ in 2D and 3D. Unless stated otherwise, we let

$$f(\boldsymbol{x}) = e^{-\frac{|\boldsymbol{x}|^2}{2\sigma^2}}, \qquad \phi_s(\boldsymbol{x}) = f(\boldsymbol{x}), \qquad \boldsymbol{x} \in \mathbb{R}^d \tag{41}$$

Algorithm 1 Simple Fast Spectral Convolution algorithm for $\widehat{\chi}_1(f)$

Comment: Given a smooth function f, ground state ϕ_s and dipole-dipole interaction Φ_s on mesh grid $\mathcal{T}_{\boldsymbol{x}}$.

Comment: Pre-compute the Fourier transform $\widehat{U}_{pq}$ (40) up to controlled tolerance ϵ.

1: Compute density $\rho =: \phi_s f$ by multiplication.
2: Compute the effective DDI-density $\widetilde{\rho}$ (35) by differentiating ρ on $\mathcal{T}_{\boldsymbol{x}}$ via Fourier spectral method.
3: Carry out a twofold zero-padding of DDI-density (denoted by $\widetilde{\rho}$).
4: Compute the discrete Fourier coefficient of $\widetilde{\rho}$ via FFT, i.e. $\widehat{\rho}_{pq}$ in (38).
5: Compute $\widehat{\rho}_{pq}\widehat{U}_{pq}$ by multiplication.
6: Compute the nonlocal potential φ (39) on $\mathcal{T}_{\boldsymbol{x}}$ via iFFT.
7: Compute $\chi_1(f) = \varphi\phi_s$ by multiplication.

and set the dipole orientation as $\boldsymbol{n} = (0.82778, 0.41505, -0.37751)^T$. We set the computational domain as $\mathcal{D} = [-8, 8]^d$ and we always use uniform (tensor) grids in space with equal mesh sizes h in all directions. To quantify the errors, we define the error function as

$$E_h =: \frac{\left\|[\chi_1(f)]_{\text{num}} - [\chi_1(f)]_{\text{exact}}\right\|_\infty}{\left\|[\chi_1(f)]_{\text{exact}}\right\|_\infty},$$

where $[\chi_1(f)]_{\text{num}}$ is the numerical solution obtained by SFSC and $[\chi_1(f)]_{\text{exact}}$ is the exact solution.

EXAMPLE 1. *With the choice of f and ϕ_s in (41), the exact interaction $\chi_1(f)$ in 2D can be given explicitly as*

$$\chi_1(f)(\boldsymbol{x}) = \frac{3\sqrt{\pi}e^{-s}}{4\sigma}\left[(\boldsymbol{n}_\perp\cdot\boldsymbol{n}_\perp)(I_0(s)-I_1(s)) - \frac{2(\boldsymbol{x}\cdot\boldsymbol{n}_\perp)^2}{\sigma^2}\Big(I_0(s)-\frac{1+2s}{2s}I_1(s)\Big)\right]f(\boldsymbol{x}) + \frac{3\sqrt{\pi}\,n_3\,n_3\,s\,e^{-s}}{\sigma}\Big[I_0(s)-I_1(s)-\frac{I_0(s)}{2\,s}\Big]f(\boldsymbol{x}),$$

where $s = \frac{|\boldsymbol{x}|^2}{2\sigma^2}$, I_0 and I_1 are the modified Bessel functions of order 0 and 1 respectively. While in 3D, we have

(42)
$$\chi_1(f)(\boldsymbol{x}) = -\left[\rho(\boldsymbol{x}) + 3\,\partial_{\boldsymbol{nn}}\left(\frac{\sigma^2\sqrt{\pi}}{4}\frac{Erf(r/\sigma)}{r/\sigma}\right)\right]f(\boldsymbol{x}) = -[\rho(\boldsymbol{x}) + 3\,\boldsymbol{n}^T B(\boldsymbol{x})\boldsymbol{n}]f(\boldsymbol{x})$$

with matrix $B(\boldsymbol{x}) = (b_{jl}(\boldsymbol{x}))_{j,l=1}^3$ defined as

(43)
$$b_{jl}(\boldsymbol{x}) = \left(\frac{\sigma^2}{2r^2}e^{-\frac{r^2}{\sigma^2}} - \frac{\sigma^3\sqrt{\pi}}{4r^3}Erf\Big(\frac{r}{\sigma}\Big)\right)\delta_{jl}$$

(44)
$$+x_j x_l\left(-e^{-\frac{r^2}{\sigma^2}}\left(\frac{3\,\sigma^2}{2\,r^4}+\frac{1}{r^2}\right) + \frac{3\sigma^3\sqrt{\pi}}{4\,r^5}Erf\Big(\frac{r}{\sigma}\Big)\right),$$

where $r = |\boldsymbol{x}|$, δ_{jl} is the Kronecker delta, $\boldsymbol{x} = (x_1, x_2, x_3)^T$ and $Erf(r) = \frac{2}{\sqrt{\pi}}\int_0^r e^{-t^2}dt$ is the error function.

For all numerical examples in this paper, the related algorithms were implemented in Fortran and run on a 2.27GH Intel(R) Xeon(R) CPU E5520 with a 8 MB cache in

Debian GNU/Linux. Table 1 shows the numerical errors E_h and corresponding CPU times by SFSC with different mesh size h for Example 1. Since the CPU time for 2D case is too small, we only present those for 3D case. From the table, we could clearly see that SFSC is efficient and achieves spectral accuracy.

TABLE 1
Errors and CPU time (in seconds) for computing the nonlocal interaction $\chi_1(f)$ by SFSC with different mesh size h in 2D (Upper) and 3D (Lower) cases in Example 1.

	$h=2$	$h=1$	$h=1/2$	$h=1/4$
E_h	1.9385E-01	1.1617E-02	7.6144E-08	3.7585E-15
E_h	1.5743E-01	8.2904E-03	1.7048E-07	1.8485E-14
CPU	6.0000E-04	5.5000E-03	5.6300E-02	9.5620E-01

4. Numerical results. In this section, we first test the convergence of the matrix-free IRAM integrated with the SFSC (SFSC-IRAM) method to solve the BdGEs (18). Then, we apply the SFSC-IRAM method to investigate the Bogoliubov excitations around the ground states of GPE. The ground states ϕ_s and chemical potential μ_s (34) are computed via the PCG-ATKM [46] in a large enough domain with small enough mesh size such that the errors coming from spatial discretization are negligible. Unless stated otherwise, we choose the potential $V(\boldsymbol{x})$ as the harmonic trapping potential (4) and set respectively the computational domain as $\mathcal{D}=[-12,12]^2$ in 2D and $\mathcal{D}=[-10,10]^3$ in 3D. We always use uniform (tensor) grids in space with equal mesh sizes h in all directions.

4.1. Accuracy tests. Here, we first test the spatial accuracy of our method in 2D and 3D. To this end, we take the same parameters as in the **Lemma 2**, which imply analytical formula for the eigenvalue and eigenvectors to the BdGEs (34). For an abstract analytical eigenvalue solution ω with multiplicity p to the BdGEs (34), we denote its associated analytical eigenvectors (as given in (25)) as $(\boldsymbol{u}_j,\boldsymbol{v}_j)$ $(j=1,\cdots,p)$, and denote the corresponding linear eigenvector space as $P_u =: \text{span}\{\boldsymbol{u}_1,\cdots,\boldsymbol{u}_p\}$ & $P_v =: \text{span}\{\boldsymbol{v}_1,\cdots,\boldsymbol{v}_p\}$. For example, as shown in **Lemma 2**, for $\gamma_x=\gamma_y=\gamma$ in 2D, $p=2$ for eigenvalue $\omega=\gamma$ and the associated eigenvectors $(\boldsymbol{u}_j,\boldsymbol{v}_j)$ $(j=1,2)$ are analytically given in (25). To demonstrate the results, we define the following error functions for eigenvalues and eigenvectors

$$e^h_{\omega_\alpha} := \frac{|\omega^h_\alpha-\omega_\alpha|}{|\omega_\alpha|}, \qquad e^{h,\alpha}_{\boldsymbol{uv}} := \frac{\|\boldsymbol{u}^h_\alpha-\mathcal{P}_u\boldsymbol{u}^h_\alpha\|_2}{\|\boldsymbol{u}^h_\alpha\|_2}+\frac{\|\boldsymbol{v}^h_\alpha-\mathcal{P}_v\boldsymbol{v}^h_\alpha\|_2}{\|\boldsymbol{v}^h_\alpha\|_2}.$$

Here, $\alpha=x,y$ in 2D and $\alpha=x,y,z$ in 3D, $\|\cdot\|_2$ is the discrete l^2 norm and $\mathcal{P}_\nu$ $(\nu=u,v)$ is the l^2-orthogonal projection operator into space P_ν. $\{\boldsymbol{u}^h_\alpha,\boldsymbol{v}^h_\alpha,\omega^h_\alpha\}$ is the numerical approximation for the eigen-pair $\{\boldsymbol{u}_\alpha,\boldsymbol{v}_\alpha,\omega_\alpha\}$ that defined by (25) in **Lemma 2**.

EXAMPLE 2. *Here, we consider both the 2D and 3D examples. To this end, we set $\beta=100$, $\lambda=50$ and consider the following four cases:*

Case I. *2D case, let $\gamma_x=\gamma_y=1$ and $\boldsymbol{n}=(\cos\theta,\sin\theta,0)^T$ with different θ.*

Case II. *2D case, let $\gamma_x=\gamma_y/2=1$ and $\boldsymbol{n}=(\cos\theta,\sin\theta,0)^T$ with different θ.*

Case III. *3D case, let $\gamma_x=\gamma_y=\gamma_z=1$ and $\boldsymbol{n}=(0,0,1)^T$.*

Case IV. *3D case, let $\gamma_x=\gamma_z=\gamma_y/2=1$ and $\boldsymbol{n}=(0,0,1)^T$.*

For **Case I**, the two analytical eigenvalues are $\omega_x = \omega_y =: \omega = 1$ hence $p = 2$ for eigenvalue $\omega = 1$ and the dimension of its generated eigenvector space P_u & P_v. While $\omega_x = 1$, $\omega_y = 2$ for **Case II**, thus both of their corresponding eigenvector space is of dimension one. Similarly, for **Case III**, the three analytical eigenvalues are $\omega_x = \omega_y = \omega_z =: \omega = 1$ hence $p = 3$ for eigenvalue $\omega = 1$ and the dimension of its associated eigenvector space P_u & P_v. While for **Case IV**, $\omega_x = \omega_y =: \omega = 1$ and $\omega_z = 2$, thus the dimension of the associated eigenvector space is two for ω and one for ω_z, respectively.

Table 2-3 illustrate the errors of eigenvalues and eigenvectors for different mesh size h and/or different dipole orientation $\boldsymbol{n}$ for **Case I**-**Case IV**. From this table, we could clearly see that the proposed method is of spectral accuracy in space.

TABLE 2
Errors of the eigenvalues/eigenvectors for **Case I** *(upper) and* **Case II** *(lower) in Example 2.*

	h	$h_0 = 3/2$	$h_0/2$	$h_0/4$	$h_0/8$	$h_0/16$
$\theta = 0$	$e^h_{\omega_x}$	1.569E-01	6.618E-04	7.652E-07	1.516E-12	1.129E-11
	$e^h_{\omega_y}$	9.973E-02	1.927E-03	6.508E-08	7.641E-13	1.129E-11
	$e^{h,\omega_x}_{\boldsymbol{uv}}$	1.993E-01	1.211E-02	2.144E-04	3.474E-08	6.107E-11
	$e^{h,\omega_y}_{\boldsymbol{uv}}$	2.068E-01	1.932E-02	2.715E-05	4.611E-09	3.938E-11
$\theta = \pi/4$	$e^h_{\omega_x}$	2.085E-01	6.525E-04	3.957E-07	1.451E-13	5.653E-12
	$e^h_{\omega_y}$	1.283E-01	1.682E-03	1.967E-07	5.680E-13	1.299E-11
	$e^{h,\omega_x}_{\boldsymbol{uv}}$	1.851E-01	1.644E-02	1.214E-04	8.606E-09	3.962E-11
	$e^{h,\omega_y}_{\boldsymbol{uv}}$	2.989E-01	1.657E-02	1.325E-04	8.822E-09	5.275E-11
$\theta = \pi/3$	$e^h_{\omega_x}$	1.889E-01	7.926E-04	1.375E-07	4.345E-13	1.637E-11
	$e^h_{\omega_y}$	1.209E-01	3.174E-03	1.234E-06	1.217E-12	7.761E-12
	$e^{h,\omega_x}_{\boldsymbol{uv}}$	1.848E-01	1.490E-02	7.475E-05	1.851E-08	6.890E-11
	$e^{h,\omega_y}_{\boldsymbol{uv}}$	2.775E-01	1.779E-02	1.679E-04	1.873E-08	2.595E-11
	h	$h_0 = 3/4$	$h_0/2$	$h_0/4$	$h_0/8$	$h_0/16$
$\theta = 0$	$e^h_{\omega_x}$	1.583E-01	2.000E-03	2.131E-06	4.209E-12	1.220E-11
	$e^h_{\omega_y}$	1.858E-02	5.973E-03	1.388E-05	9.854E-13	9.976E-12
	$e^{h,\omega_x}_{\boldsymbol{uv}}$	4.431E-01	2.076E-02	2.421E-04	8.561E-08	5.781E-11
	$e^{h,\omega_y}_{\boldsymbol{uv}}$	2.000	7.879E-02	8.098E-04	8.165E-08	5.241E-11
$\theta = \pi/4$	$e^h_{\omega_x}$	2.168E-01	3.823E-03	3.399E-06	1.854E-11	1.004E-11
	$e^h_{\omega_y}$	1.215E-01	3.346E-02	1.104E-04	4.233E-10	3.712E-12
	$e^{h,\omega_x}_{\boldsymbol{uv}}$	5.428E-01	2.272E-02	1.931E-04	4.903E-08	1.565E-10
	$e^{h,\omega_y}_{\boldsymbol{uv}}$	2.000	1.022E-01	2.049E-03	1.910E-06	1.962E-10
$\theta = \pi/3$	$e^h_{\omega_x}$	2.251E-01	3.529E-04	7.674E-06	2.561E-11	4.069E-12
	$e^h_{\omega_y}$	1.553E-01	5.355E-03	1.755E-04	1.225E-09	6.111E-13
	$e^{h,\omega_x}_{\boldsymbol{uv}}$	4.452E-01	2.279E-02	1.768E-04	6.936E-08	5.168E-10
	$e^{h,\omega_y}_{\boldsymbol{uv}}$	2.000	1.014E-01	2.808E-03	3.584E-06	5.872E-11

4.2. Applications. In this section, we show some applications of the SFSC-IRAM method to compute the Bogoliubov excitations around the ground state of the GPE with different parameters in 2D/3D. We investigate the effect of trapping potential, dipole orientation and local/nonlocal interaction strength on the solutions

TABLE 3
Errors of the eigenvalue/eigenvector for **Case III** *(upper) and* **Case IV** *(lower) in Example 2.*

	$h_0 = 4/5$	$h_0/2$	$h_0/4$	$h_0/8$
$e^h_{\omega_x}$	3.948E-02	2.623E-04	3.119E-11	4.456E-11
$e^h_{\omega_y}$	1.564E-02	1.463E-05	2.832E-11	1.334E-12
$e^h_{\omega_z}$	1.564E-02	1.463E-05	1.402E-09	9.087E-12
$e^{h,\omega_x}_{\boldsymbol{uv}}$	1.502E-01	5.478E-03	2.628E-07	6.311E-10
$e^{h,\omega_y}_{\boldsymbol{uv}}$	1.356E-01	2.047E-03	2.628E-07	1.753E-10
$e^{h,\omega_z}_{\boldsymbol{uv}}$	1.356E-01	2.047E-03	2.628E-07	1.753E-10
	$h_0 = 3/2$	$h_0/2$	$h_0/4$	$h_0/8$
$e^h_{\omega_x}$	1.256E-01	1.323E-03	2.963E-08	3.394E-10
$e^h_{\omega_y}$	1.049E-02	6.551E-03	1.885E-06	2.984E-11
$e^h_{\omega_z}$	1.704E-02	4.007E-04	2.352E-07	4.285E-11
$e^{h,\omega_x}_{\boldsymbol{uv}}$	3.592E-01	1.105E-02	1.216E-05	1.349E-09
$e^{h,\omega_y}_{\boldsymbol{uv}}$	2.000	1.240E-01	5.009E-04	8.537E-09
$e^{h,\omega_z}_{\boldsymbol{uv}}$	2.660E-01	1.616E-02	6.010E-05	3.409E-10

to BdGEs. To this end, we fix $h = 1/8$ and study the following examples in 2D/3D. We will only illustrate the results for the first few smallest positive eigenvalues and the associated eigenvectors.

EXAMPLE 3. *Here, we consider the effect of the interaction strength to the eigenvalues of the BdGEs with symmetric/asymmetric harmonic potentials in 2D. To this end, we study the following four cases:*

Case I. *Let* $\gamma_x = \gamma_y = 1$, $\beta = 500$ *and* $\boldsymbol{n} = (0, 0, 1)^T$. *Vary* λ *from -400 to 0.*

Case II. *Let* $\gamma_x = \gamma_y = 1$, $\lambda = -100$ *and* $\boldsymbol{n} = (0, 0, 1)^T$. *Vary* β *from 0 to 400.*

Case III. *Let* $\gamma_x = 1$, $\gamma_y = \pi$, $\beta = 500$ *and* $\boldsymbol{n} = (1, 0, 0)^T$. *Vary* λ *from 0 to 800.*

Case IV. *Let* $\gamma_x = 1$, $\gamma_y = \pi$, $\lambda = 100$ *and* $\boldsymbol{n} = (1, 0, 0)^T$. *Vary* β *from 0 to 800.*

Figure 1 shows the nine smallest positive eigenvalues ω_ℓ ($\ell = 1, \cdots, 9$) for **Case I**-**Case IV**. From this figure, we can see that: (i) For **Case I** and **Case II**, the lowest eigenvalues $\omega_1 = \omega_2$ do not change with the interaction, which indicates that the lowest dipole mode in an external harmonic potential, corresponding to a rigid motion of the center of mass, is independent of the nature of interatomic forces [20, 44]. In addition, for any interaction parameter β & λ, the Bogoliubov eigenvalue $\omega_1 = \omega_2 = 1$ agrees well with **Lemma** 2. Moreover, we observe that the multiplicity of eigenvalue ω_7 is one, and the multiplicity of $\omega_1, \omega_3, \omega_5$ and ω_8 is two. (ii) For **Case III** and **Case IV**, there exist the Bogoliubov eigenvalues $\omega_j = 1, \pi$ for any β & λ. As the interaction strength changes, there is an order-exchange between the fourth and fifth eigenvalue with one of them being π, and the changing point is $\lambda \approx 251.24$ for **Case III** and $\beta \approx 275.10$ for **Case IV**. The order-exchange corresponds to excitation energy degeneracy, and it may also occur for other eigenvalues, e.g. between ω_7 and ω_8 in both **Case III** and **Case IV**. The physical mechanism behind is quite complicated and nontrivial, especially when it happens in higher modes. Hence we shall leave it as future work.

EXAMPLE 4. *Here, we consider the effect of the dipole orientation* $\boldsymbol{n}$ *to the Bogoliubov amplitudes* $(\boldsymbol{u}, \boldsymbol{v})$ *of the BdGEs with symmetric/asymmetric harmonic potentials*

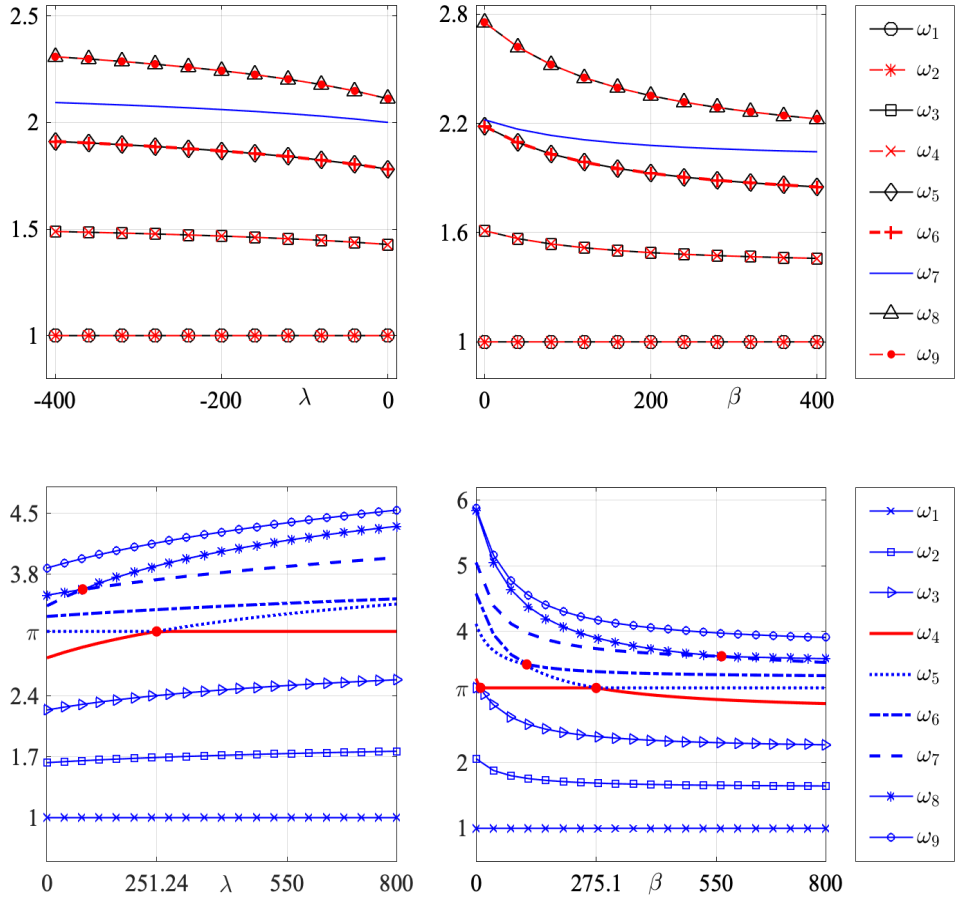

FIG. 1. *The nine smallest eigenvalues* ω_ℓ $(\ell = 1, \cdots, 9)$ *of the BdGEs for* **Case I-Case IV** *(from top left to bottom right) in Example 3.*

in 2D. To this end, we let $\beta = 500$, $\lambda = 400$ *and study the following three cases:*

Case I. $\gamma_x = \gamma_y = 1$, $\boldsymbol{n} = (1, 0, 0)^T$.

Case II. $\gamma_x = \gamma_y = 1$, $\boldsymbol{n} = (\sqrt{2}/2, \sqrt{2}/2, 0)^T$.

Case III. $\gamma_x = 1$, $\gamma_y = \pi$, $\boldsymbol{n} = (1, 0, 0)^T$.

Figures 2 displays the numerical solutions $(\boldsymbol{u}_\ell, \boldsymbol{v}_\ell)$ of the BdGEs that are associated with the first four positive eigenvalues ω_ℓ $(\ell = 1, 2, 3, 4)$ for **Case I-Case III**. From this figure we can see that both the dipole orientation and external potential affect the shape of the eigenvector $(\boldsymbol{u}_\ell, \boldsymbol{v}_\ell)$ essentially and significantly. The eigenvectors $(\boldsymbol{u}_\ell, \boldsymbol{v}_\ell)$ $(\ell = 1, 2, 3, 4)$ are symmetric or anti-symmetric along the dipole orientation in a symmetric external potential. Meanwhile the eigenvectors will be compressed along the direction with larger trapping frequency. Indeed, the presences of DDI and anisotropic external potential bring much more rich phase diagrams for eigenmodes of BdGEs, which will be detailed in future.

EXAMPLE 5. *Here, we consider the 3D case. We fixed* $\beta = 100, \lambda = 90$ *and study*

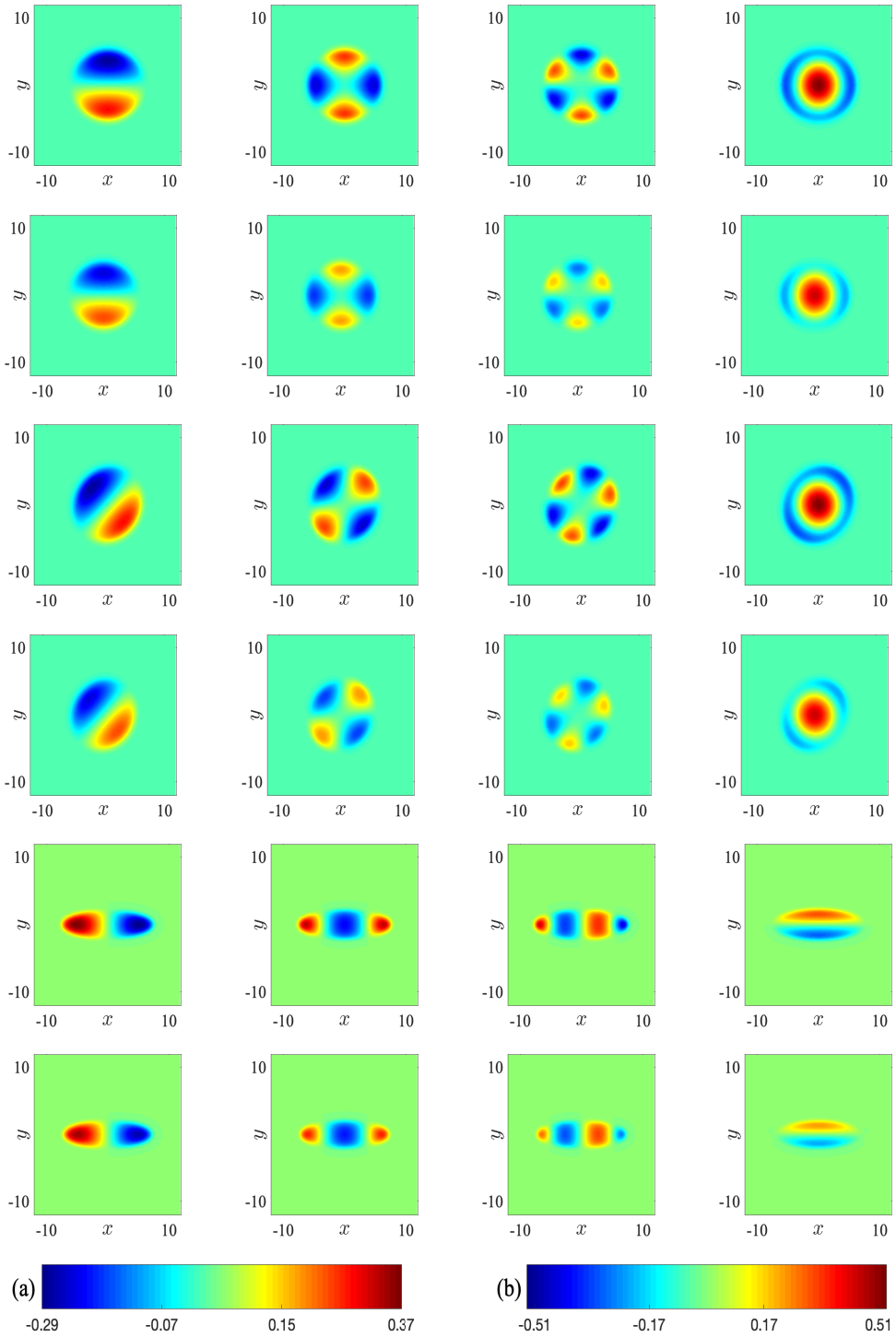

FIG. 2. *Contour plots of the Bogoliubov amplitudes* $(\boldsymbol{u}_\ell, \boldsymbol{v}_\ell)$ $(\ell = 1, \cdots, 4)$ *in Example 4 for* **Case I** *(the first two rows),* **Case II** *(the 3rd and 4th row) and* **Case III** *(the last two rows) with odd rows for* $\boldsymbol{u}_\ell$ *and even rows for* $\boldsymbol{v}_\ell$ *(from left to right* $\ell = 1, \cdots, 4$*) as well as the colorbars for* **Case I-Case II (a)** *and* **Case III (b)**.

the following two cases:

Case I. *Symmetric potential:* $\gamma_x = \gamma_y = \gamma_z = 1$. *Let* $\boldsymbol{n} = (1, 0, 0)^T$.

Case II. *Asymmetric potential:* $\gamma_x = \gamma_z = 1$, $\gamma_y = 2$. *Let* $\boldsymbol{n} = (0, 0, 1)^T$.

Figure 3 shows the isosurface plots of the eigenvectors $(\boldsymbol{u}_\ell, \boldsymbol{v}_\ell) = (10^{-3}, 10^{-3})$ $(\ell = 1, \cdots, 4)$ that are associated with the first four smallest positive eigenvalues ω_ℓ $(\ell = 1, \cdots, 4)$ for **Case I**. While figure 4 shows those associated with the first five smallest eigenvalues for **Case II**. Note that the multiplicity of $\omega_1 = 1$ is three and two for **Case I** and **Case II** respectively, hence there exists three (two) independent eigenvectors for **Case I** (**Case II**). Here we only present $(\boldsymbol{u}_1, \boldsymbol{v}_1)$ simply because the other modes are quite similar. Similarly as the 2D cases, we could see that both the dipole orientation ands external potential affect the shape of the eigenvectors essentially and significantly. The eigenvectors $(\boldsymbol{u}_\ell, \boldsymbol{v}_\ell)$ $(\ell = 1, 2, 3, 4)$ are (anti)symmetric along the dipole orientation in a symmetric external potential, and the eigenfunctions is more compressed in the stronger trapping direction.

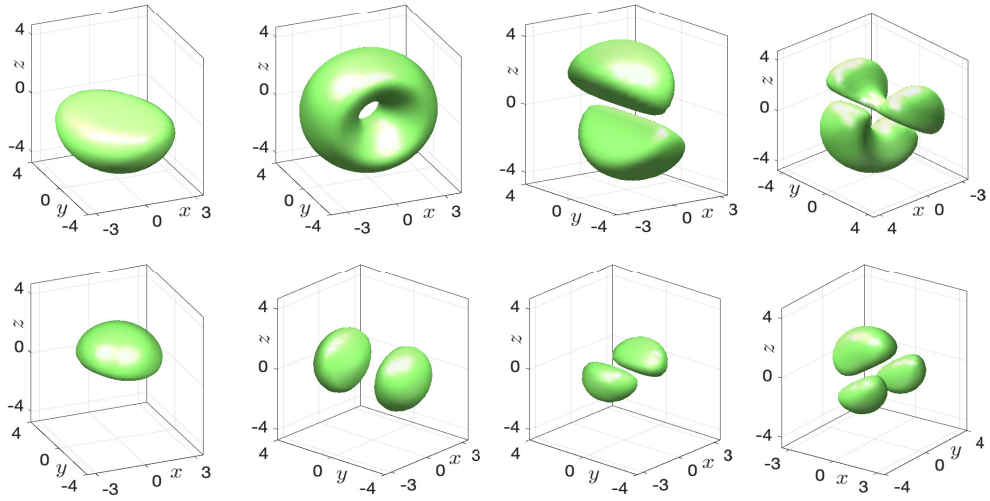

FIG. 3. *Isosurface plots of the Bogoliubov amplitude of* $\boldsymbol{u}_\ell = 10^{-3}$ *(upper),* $\boldsymbol{v}_\ell = 10^{-3}$ *(lower) (left to right:* $\ell = 1, \cdots, 4$*) for* **Case I** *in Example 5.*

5. Conclusion. We proposed an efficient spectrally accurate method to compute the Bogoliubov-de Gennes equations (with nonlocal dipole-dipole interaction term) characterizing the elementary excitations of dipolar BEC. Combining together the Fourier spectral method for spatial discretization, the Simple Fourier Spectral Convolution method for evaluation of the nonlocal dipole-dipole interaction and the matrix-free IRAM method for the discrete eigenvalue problem, the proposed method is numerically confirmed to be highly efficient (with $O(N \log N)$ operations) and of spectral accuracy. We then apply our method to investigate the effect of various parameters, including the external trapping potential, the interaction strength and the dipole orientation to the Bogoliubov excitations in both two and three dimensions. The corresponding distributions of excitation spectrum are illustrated and the Bogoliubov amplitudes are also presented. In addition, we obtained analytically the first few nontrivial eigenvalues and the associated eigenvectors when the harmonic potentials is employed. Our proposed methods could be easily extended to investi-

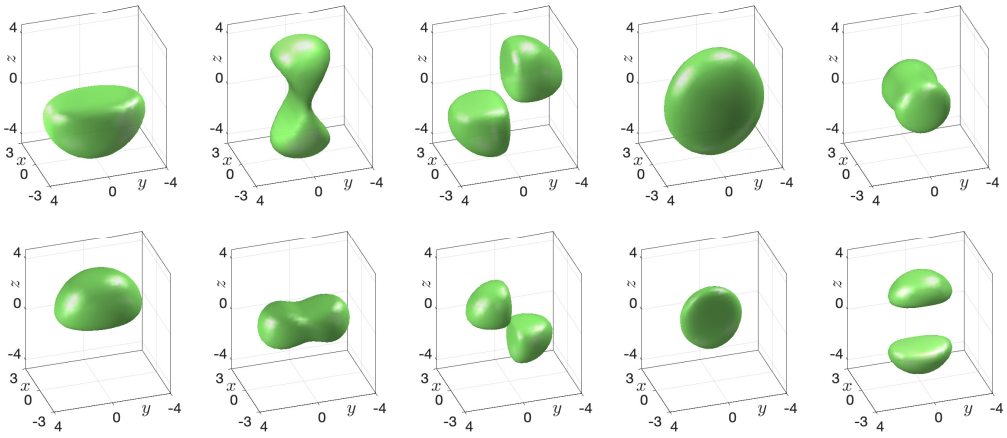

FIG. 4. *Isosurface plots of the Bogoliubov amplitude of* $\boldsymbol{u}_\ell = 10^{-3}$ *(upper),* $\boldsymbol{v}_\ell = 10^{-3}$ *(lower) (left to right:* $\ell = 1, \cdots, 5$*) for* **Case II** *in Example 5.*

gate the excitation spectrums for other systems such as the rotating dipolar BEC and spinor-dipolar BEC, and we shall report them in our future work.

Acknowledgements. This work was partially done while Yong Zhang and Q. Tang were visiting the Institute for Mathematical Sciences, National University of Singapore in 2020.

REFERENCES

[1] Advanpix multiprecision computing toolbox. https://www.advanpix.com

[2] K. Aikawa, A. Frisch, M. Mark, S. Baier, A. Rietzler, R. Grimm and F. Ferlaino, *Bose-Einstein Condensation of Erbium*, Phys. Rev. Lett., **108** (2012), article 210401.

[3] X. Antoine and R. Duboscq, *Robust and efficient preconditioned Krylov spectral solvers for computing the ground states of fast rotating and strongly interacting Bose-Einstein Condensates*, J. Comput. Phys., **258** (2014), 509-523.

[4] X. Antoine, A. Levitt and Q. Tang, *Efficient spectral computation of the stationary states of rotating Bose-Einstein condensates by preconditioned nonlinear conjugate gradient methods*, J. Comput. Phys., **343** (2017), 92-109.

[5] X. Antoine, Q. Tang and Y. Zhang, *A Preconditioned Conjugated Gradient Method for computing ground sates of rotating dipolar Bose-Einstein condensates via Kernel Truncation Method for Dipole-Dipole Interaction evaluation*, Commun. Comput. Phys., **24** (4) (2018), 966-988.

[6] Z. Bai and R. C. Li, *Minimization principles for the linear response eigenvalue problem I: Theory*, SIAM J. Matrix Anal. Appl., **33** (4) (2012), 1075-1100.

[7] Z. Bai and R.C. Li, *Minimization principles for linear response eigenvalue problem II: Computation*, SIAM J. Matrix Anal. Appl., **34** (2) (2013), 392-416.

[8] D. Baillie, R. M. Wilson and P. B. Blakie, *Collective excitations of self-bound droplets of a dipolar quantum fluid*, Phys. Rev. Lett., **119** (25) (2017), article 255302.

[9] W. Bao and Y. Cai, *Mathematical theory and numerical methods for Bose-Einstein condensation*, Kinet. Relat. Mod., **6** (2013), 1-135.

[10] W. Bao, Y. Cai and H. Wang, *Efficient numerical methods for computing ground states and dynamics of dipolar Bose-Einstein condensates*, J. Comput. Phys., **229** (2010), 7874-7892.

[11] W. Bao, I. Chern and F. Y. Lim, *Efficient and spectrally accurate numerical methods for computing ground and first excited states in Bose-Einstein condensates*, J. Comput. Phys., **219** (2006), 836-854.

[12] W. Bao, H. Jian, N. J. Mauser and Y. Zhang, *Dimension reduction of the Schrödinger equation with coulomb and anisotropic confining potentials*, SIAM J. Appl. Math., **73** (6) (2013), 2100-2123.
[13] W. Bao, S. Jiang, Q. Tang and Y. Zhang, *Computing the ground state and dynamics of the nonlinear Schrödinger equation with nonlocal interactions via the nonuniform FFT*, J. Comput. Phys., **296** (2015), 72-89.
[14] W. Bao, Q. Tang and Y. Zhang, *Accurate and efficient numerical methods for computing ground states and dynamics of dipolar Bose-Einstein condensates via the nonuniform FFT*, Commun. Comput. Phys., **19** (5) (2016), 1141-1166.
[15] W. Bao, L. Treust and F. Mehats, *Dimension reduction for dipolar Bose-Einstein condensates in the strong interaction regime*, Kinet. Relat. Mod., **10** (2017), 553-571.
[16] M.A. Baranov, *Theoretical progress in many-body physics with ultracold dipolar gases*, Physics Reports, **464** (2008), 71-111.
[17] Y. Cai, M. Rosenkranz, Z. Lei and W. Bao, *mean field regime of trapped dipolar Bose-Einstein condensates in one and two dimensions*, Phys. Rev. A, **82** (2010), article 043623.
[18] I. Danaila and F. Hecht, *A finite element method with mesh adaptivity for computing vortex states in fast-rotating Bose-Einstein condensates*, J. Comput. Phys., **229** (2010), 6946-6960.
[19] I. Danaila, M. A. Khamehchi, V. Gokhroo, P. Engels and P. G. Kevrekidis, *Vector dark-antidark solitary waves in multicomponent Bose-Einstein condensates*, Phys. Rev. A, **94** (5) (2016), article 053617.
[20] M. Edwards, P. A. Ruprecht, K. Burnett, R. J. Dodd and C. W. Clark, *Collective excitations of atomic Bose-Einstein condensates* Phys. Rev. Lett., **77** (9) (1996) 1671-1674.
[21] L. Exl, N. J. Mauser and Y. Zhang, *Accurate and efficient computation of nonlocal potentials based on Gaussian-sum approximation*, J. Comput. Phys., **327** (2016), 629-642.
[22] C. Eberlein, S. Giovanazzi and D. H. G. O'Dell, *Exact solution of the Thomas-Fermi equation for a trapped Bose-Einstein condensate with dipole-dipole interactions*, Phys. Rev. A, **71** (3) (2005), article 033618.
[23] I. Ferrier-Barbut, H. Kadau, M. Schmitt, M. Wenzel and T. Pfau, *Observation of quantum droplets in a strongly Dipolar Bose gas*, Phys. Rev. Lett., **116** (2016), article 215301.
[24] Y. Gao and Y. Cai, *Numerical methods for Bogoliubov-de Gennes excitations of Bose-Einstein condensates*, J. Comput. Phys., **403** (2020), article 109058.
[25] L. Greengard, S. Jiang and Y. Zhang, *The anisotropic truncated kernel method for convolution with free-space Green's functions*, SIAM J. Sci. Comput., **38** (2018), A3733-A3754.
[26] K. Góral, K. Rzayewski and T. Pfau, *Bose-Einstein condensation with magnetic dipole-dipole forces*, Phys. Rev. A, **61** (2000), article 051601(R).
[27] A. Griesmaier, J. Werner, S. Hensler, J. Stuhler and T. Pfau, *Bose-Einstein condensation of Chromium*, Phys. Rev. Lett., **94** (2005), article 160401.
[28] B. Hu, G. Huang and Y. L. Ma, *Analytical solutions of the Bogoliubov-de Gennes equations for excitations of a trapped Bose-Einstein-condensed gas*, Phys. Rev. A, **69** (6) (2004), article 063608.
[29] L. Jia, A.-B. Wang and S. Yi, *Low-lying excitations of vortex lattices in condensates with anisotropic dipole-dipole interaction*, Phys. Rev. A, **97** (2018), article 043614.
[30] S. Jia, H. Xie, M. Xie and F. Xu, *A full multigrid method for nonlinear eigenvalue problems*, Sci. China Math., **59** (10) (2016), 2037-2048.
[31] S. Jiang, L. Greengard and W. Bao, *Fast and accurate evaluation of nonlocal Coulomb and dipole-dipole interactions via the nonuniform FFT*, SIAM J. Sci. Comput., **36** (2014), B777-B794.
[32] D. S. Jin, J. R. Ensher, M. R. Matthews, C. E. Wieman and E. A. Cornell, *Collective Excitations of a Bose-Einstein Condensate in a Dilute Gas*, Phys. Rev. Lett., **77** (1996), 420-423.
[33] H. Kadau, M. Schmitt, M. Wenzel, C. Wink, T. Maier, I. Ferrier-Barbut and T. Pfau, *Observing the Rosensweig instability of a quantum ferrofluid*, Nature, **530** (2016), 194-197.
[34] P. G. Kevrekidis and D. E. Pelinovsky, *Distribution of eigenfrequencies for oscillations of the ground state in the Thomas-Fermi limit*, Phys. Rev. A, **81** (2)

(2010), article 023627.
[35] T. Lahaye, C. Menotti, L. Santos, M. Lewenstein and T. Pfau, *The physics of dipolar bosonic quantum gases*, Rep. Prog. Phys., **72** (2009), article 126401.
[36] T. Lahaye, J. Metz, B. Fröhlich, T. Koch, M. Meister, A. Griesmaier, T. Pfau, H. Saito, Y. Kawaguchi and M. Ueda, *D-wave collapse and explosion of a dipolar Bose-Einstein condensate*, Phys. Rev. Lett., **101** (2008), article 080401.
[37] A. J. Leggett, *Bose-Einstein condensation in the alkali gases: Some fundamental concepts*, Rev. Mod. Phys., **73** (2001), 307-356.
[38] M. Lu, N. Q. Burdick, S. H. Youn and B. L. Lev, *Strongly dipolar Bose-Einstein condensate of Dysprosium*, Phys. Rev. Lett., **107** (2011), article 190401.
[39] A. M. Martin, N. G. Marchant, D. H. J. O'Dell and N. G. Parker, *Vortices and vortex lattices in quantum ferrofluids*, J. Phys.: Condens. Matter, **29** (2017), article 103004.
[40] S. A. Morgan, S. Choi, K. Burnett and M. Edwards, *Nonlinear mixing of quasi-particles in an inhomogeneous Bose condensate*, Phys. Rev. A, **57** (1998), article 3818.
[41] S. Ronen, D. C. E. Bortolotti and J. L. Bohn, *Bogoliubov modes of a dipolar condensate in a cylindrical trap*, Phys. Rev. A, **74** (2006), article 013623.
[42] C. A. Rozzi, D. Varsano, A. Marini, E. K. U. Gross and A. Rubio, *Exact coulomb cutoff technique for supercell calculations*, Phys. Rev. B, **73** (20) (2006), article 205119.
[43] Y. Saad, *Numerical Methods for Large Eigenvalue Problems*, Society for Industrial and Applied Mathematics, 2011.
[44] S. Stringari, *Collective excitations of a trapped Bose-condensed gas*, Phys. Rev. Lett., **77** (12) (1996), 2360-2363.
[45] M. Schmitt, M. Wenzel, F. Böttcher, I. Ferrier-Barbut and T. Pfau, *Self-bound droplets of a dilute magnetic quantum liquid*, Nature, **539** (2016), 259-262.
[46] Q. Tang, H. Wang, S. Zhang and Y. Zhang, *An efficient anisotropic method for computing the ground state and dynamics of the rotating dipolar BEC*, in preparation.
[47] The ARPACK homepage. https://www.caam.rice.edu/software/ARPACK/
[48] F. Vico, L. Greengard and M. Ferrando, *Fast convolution with free-space green's functions*, J. Comput. Phys., **323** (2016), 191-203.
[49] H. Wang, *A projection gradient method for computing ground state of spin-2 Bose-Einstein condensates*, J. Comput. Phys., **274** (2014), 473-488.
[50] R. Wilson, S. Ronen and J. L. Bohn, *Stability and excitations of a dipolar Bose-Einstein condensate with a vortex*, Phys. Rev. A, **79** (2009), article 013621.
[51] X. Wu, Z. Wen and W. Bao, *A regularized Newton method for computing ground states of Bose-Einstein condensates*, J. Sci. Comput., **73** (2017), 303-329.
[52] H. Xie and M. Xie, *A multigrid method for ground state solution of Bose-Einstein condensates*, Commun. Comput. Phys., **19** (3) (2016), 648-662.
[53] S. Yi and L. You, *Trapped condensates of atoms with dipole interactions*, Phys. Rev. A, **63** (2001), article 053607.